

Article

Numerical Investigation on Comparison of Electromagnetic Forming and Drawing for Electromagnetic Forming Characterization

Mirae Lim ¹, Hanbi Byun ¹, Yunjun Song ², Jungsoo Park ² and Jeong Kim ^{1,*} 

¹ Department of Aerospace Engineering, Pusan National University, Busan 46241, Korea; alfpeh9452@pusan.ac.kr (M.L.); hbbyun96@pusan.ac.kr (H.B.)

² Virtual Manufacturing Engineering Team, Hyundai Motor Group, Seoul 18280, Korea; yjsong01@hyundai.com (Y.S.); jsupark@hyundai.com (J.P.)

* Correspondence: greatkj@pusan.ac.kr

Abstract: Due to environmental regulations, vehicle weight reduction technology has recently emerged as a key factor influencing market competitiveness in the automobile industry. Although the demand for aluminum alloy for vehicle weight reduction is increasing, its application in the automobile industry is limited due to its low formability. Electromagnetic forming (EMF) technology has been proposed as a method to improve the low formability of aluminum alloys. EMF is a technology of forming a metal workpiece at high speed without physical contact by applying a strong electromagnetic field to the workpiece to be formed. In this study, we performed an analytical study on the characteristics of electromagnetic forming. Finite element analysis was performed with the same model as in the general drawing process, and the results of the forming process, formability, and finite element analysis were compared. Through the results of finite element analysis, it was confirmed that the EMF process showed significant deformation at the die shoulder and center. Furthermore, EMF has an advantage in formability due to having a smaller amount of sheet inflow than the drawing process; however, its forming accuracy is low.

Keywords: electromagnetic forming; deep-drawing process; finite element analysis; formability; forming limit diagram



Citation: Lim, M.; Byun, H.; Song, Y.; Park, J.; Kim, J. Numerical Investigation on Comparison of Electromagnetic Forming and Drawing for Electromagnetic Forming Characterization. *Metals* **2022**, *12*, 1248. <https://doi.org/10.3390/met12081248>

Academic Editors: Jingwei Zhao, Zhengyi Jiang, Leszek Adam Dobrzański, Chong Soo Lee and Hardy Mohrbacher

Received: 9 June 2022

Accepted: 21 July 2022

Published: 25 July 2022

Publisher's Note: MDPI stays neutral with regard to jurisdictional claims in published maps and institutional affiliations.



Copyright: © 2022 by the authors. Licensee MDPI, Basel, Switzerland. This article is an open access article distributed under the terms and conditions of the Creative Commons Attribution (CC BY) license (<https://creativecommons.org/licenses/by/4.0/>).

1. Introduction

Recently, with the automobile industry entering the era of eco-friendly vehicles such as electric and hybrid vehicles owing to regulations on carbon dioxide (CO₂) emissions and fuel efficiency, vehicle weight reduction technology has emerged as a key factor in determining market competitiveness. The demand for aluminum alloy as a lightweight structural metal instead of steel for vehicle weight reduction has increased, and many automobile companies are applying aluminum alloy to the car body [1–3]. However, due to the low formability of aluminum alloy, its scope of application in the automobile industry is limited. Electromagnetic forming (EMF) technology has been proposed as a method to improve the low formability of aluminum alloys.

EMF is a high-speed forming technology. A metal workpiece is formed by applying a strong electromagnetic field at a high speed (15–300 m/s) without any physical contact [4]. For a short time (50–200 μs), the electrical energy is instantaneously discharged to the forming coil, thereby generating an induced current in the metal workpiece. This creates Lorentz's force, which acts as a forming force on the metal workpiece. EMF has numerous advantages compared with sheet metal forming (SMF) processes such as the conventional quasi-static drawing process. Firstly, as EMF is performed without contact with the punch, it is an environmentally friendly process technology that does not require a lubricant. Secondly, as EMF is a process that does not require a punch, there is no wear caused by the

contact between the die and the punch; hence, the number of die replacements cost can be reduced [5]. Thirdly, as mentioned before, the formability of alloys increases due to high strain rates [6,7]. There are three main factors that contribute to the increase in formability in EMF. Strain rate hardening (because of high strain rate) and inertia to maintain the current state of motion as the forming is performed for a very short time are two of them. In addition, during EMF, formability is improved by reducing the void volume of the workpiece owing to the interaction between the mold and workpiece [8]. By comparing the formability of the conventional press process, drawing process, and EMF, this study intends to confirm the improvement in formability with EMF compared with the general forming method.

To study the improvement of EMF, Chen et al. [9] analyzed the dual-coil system in which coils were applied one by one above and next to the workpiece, and Kamal and Daehn [10] added a conductor to the structure of a typical EMF to deliver uniform pressure to the workpiece. Furthermore, Demir et al. performed experiments to obtain a forming limit diagram (FLD) through EMF and studied the reasons for higher FLD than the drawing process [11]. As such, studies on the application of EMF are actively conducted. However, research on how to perform EMF and identify its characteristics is insufficient. Therefore, in this study, as a basic step to apply the EMF to automotive parts in the future, the process of EMF is examined in detail using finite element analysis, thereby providing insights into the characteristics of EMF.

2. Finite Element Analysis Model

To compare the finite element analysis results of the EMF and drawing process, finite element analysis was performed using LS-DYNA of Livermore Software Technology Corporation (LSTC). The finite element analysis model was a square cup model of 50 mm × 20 mm and is shown in Figure 1. A total of four models were selected for the shape in which the fracture occurred in the drawing process. This was to confirm whether EMF has an advantage in formability over the drawing process. Parameters for each finite element analysis model are summarized and listed in Table 1. The parameters are illustrated in Figure 1. Die R is the die shoulder radius; punch R denotes punch nose radius or die corner radius, and depth implies the depth of the die.

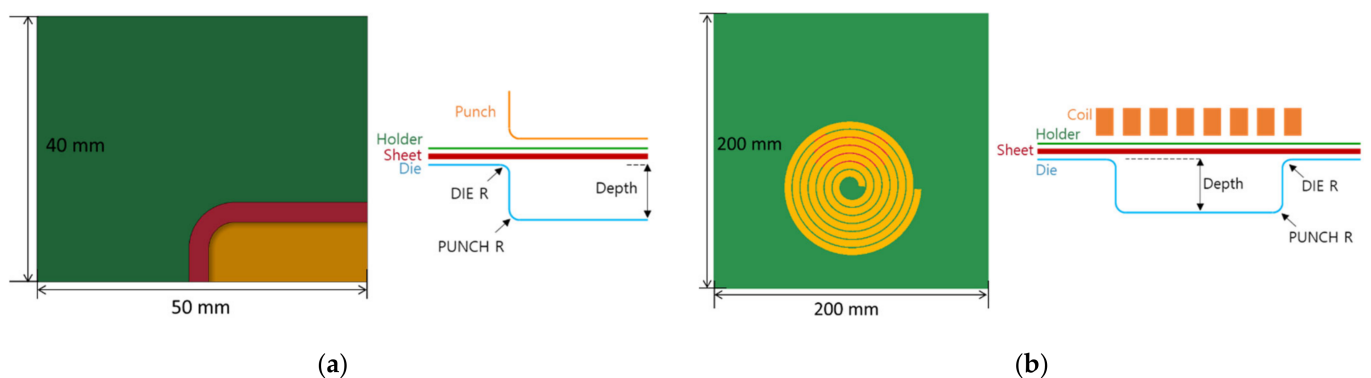


Figure 1. Finite element analysis model of (a) drawing process and (b) electromagnetic forming (EMF).

Table 1. Design parameters for die.

	Die R (mm)	Punch R (mm)	Depth (mm)
CASE 1	2	1	5
CASE 2	1	1	4
CASE 3	0.5	0.5	3
CASE 4	0.5	0.5	2

In the drawing process, as shown in Figure 1a, a 1/4 model was applied to reduce the time required for analysis, and a shell element was applied to the sheet. In LS-DYNA, the electromagnetic module only provides symmetry to the circle, and the EMF analysis model was applied the entire model, as shown in Figure 1b. The forming coil had a cross-section of 50 mm², width of 5 mm, and height of 10 mm, and the number of turns of the coil was 7. In addition, the diameter of the dead zone was approximately 14 mm. To apply the forming force to the entire forming area, a dead zone in which no electromagnetic force is generated in the forming coil was positioned outside the forming area. In addition, to avoid the boundary effect during the forming process, the size of the model was increased to 200 mm × 200 mm. This compared and analyzed only the forming by the forming coil while minimizing the effect on the forming result by concentrating the current on the edge of the sheet. A solid element was applied to the sheet for EMF analysis. This is because, in the electromagnetic molding analysis using LS-DYNA, the analysis time for solid elements was shorter than that for shell elements. Molds other than sheets were set as rigid bodies. Shell elements were applied to the die, holder, and punch, and solid elements were applied to the forming coil. The friction coefficient between the parts was 0.15, and the holding force was set to 4 tonf. Spring back was not considered in the both processes.

Copper CW004A and aluminum 6014-T4 were used as the materials for the forming coil and sheet, respectively, and the properties of these materials are summarized in Table 2. In addition, Table 3 summarizes the important factors of electromagnetic shaping, such as resistance, inductance, capacitor capacity, and input voltage.

Table 2. Material properties of copper CW004A [12] and Al 6014-T4.

Material	Property	Value
Copper CW004A	Density (kg/m ³)	7940
	Young's modulus (GPa)	117
	Poisson ratio	0.35
	Electrical conductivity (S/m)	5.85 × 10 ⁷
Al 6014-T4	Density (kg/m ³)	2680
	Young's modulus (GPa)	70
	Poisson ratio	0.30
	Electrical conductivity (S/m)	3.07 × 10 ⁷

Table 3. Current circuit parameters of EMF.

Resistance (Ω)	Inductance (H)	Capacitor (F)	Input Voltage (kV)
0.01	2.27 × 10 ⁻⁶	333 × 10 ⁻⁶	30

When performing EMF analysis, the dynamic properties of the materials due to high-speed deformation of the plate should be considered. In this study, dynamic properties for Al6014-T4 of 1 mm thickness and 250 × 250 mm² size were obtained using the inverse parameter estimation method that used the artificial neural network, as reported in [13,14]. For this, the Cowper–Symonds model (Equation (1)) was used, and the final height was designated as the standard as a result of the experiment for input voltage values of 6 kV, 7 kV and 8 kV.

$$\bar{\sigma} = \sigma_y \left[1 + \left(\frac{\dot{\epsilon}}{C} \right)^{1/p} \right] \quad (1)$$

where $\bar{\sigma}$ is the true stress, σ_y is the initial flow stress without considering the strain rate, $\dot{\epsilon}$ is the effective plastic strain rate, and C and p are the coefficients of the strain rate. Arbitrary values were assigned to C and p and applied as input to the electromagnetic finite element analysis model, with the z-axis displacement of the finite element analysis result designated

as the target value to construct a surrogate model. Through the constructed surrogate model and genetic algorithm, which is one of the optimal techniques, C and p values with the smallest error compared with the z-axis displacement of the experimental result were obtained. In this work, C was 134.8 and p was 4.355. By applying the obtained C and p to the Cowper–Symonds model, dynamic properties were obtained considering the strain rate. Figure 2 compares the z-axis displacement obtained by the numerical method and the z-axis displacement obtained through the experiment. The properties of the material obtained by the numerical method are shown in Figure 3, and this was applied to the finite element analysis. From the figure, it can be seen that as the strain value increased, both the true stress–strain curve and FLD increased. Through this, it can be predicted that formability can be improved in high-speed forming.

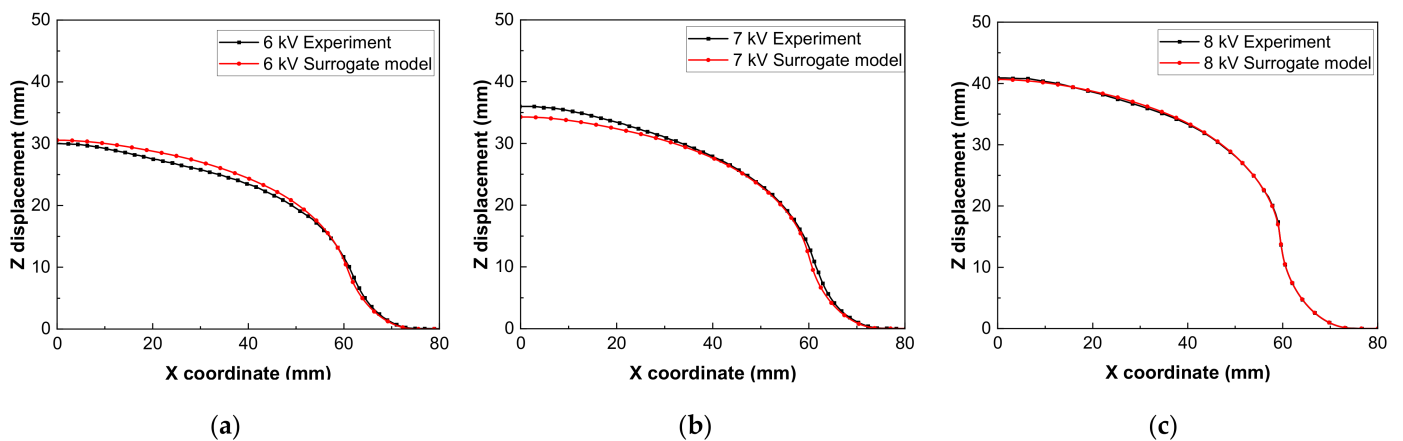


Figure 2. Comparison results of experiment and surrogate model (a) 6 kV, (b) 7 kV, and (c) 8 kV.

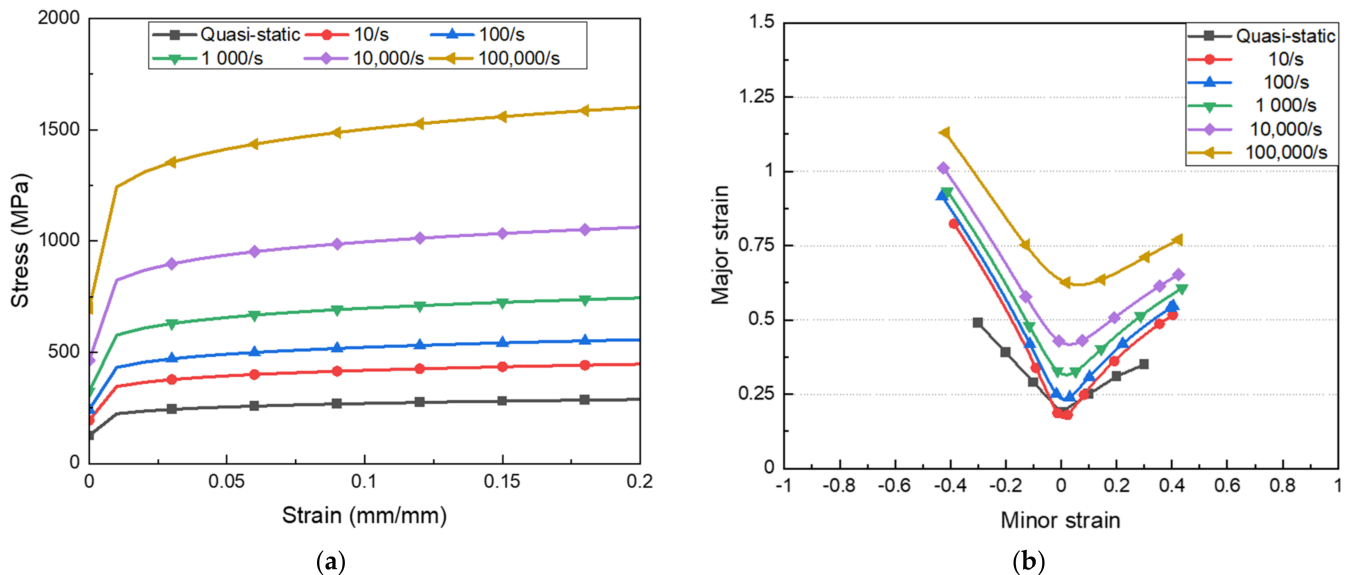


Figure 3. Dynamic properties of Al 6014-T4: (a) true stress–strain curve, (b) forming limit diagram (FLD).

3. Finite Element Analysis Results

The formability of each process was evaluated through the FLD corresponding to each process of the drawing process and EMF. In addition, by comparatively analyzing the forming processes, the cause of the predicted fracture range in each process was analyzed.

3.1. Drawing Process

The final thickness and formability evaluation are shown in Figures 4 and 5, respectively. Moreover, by calculating the final distance between the die and sheet, the accuracy,

that is, the coincidence rate with the target shape, was determined. This can be confirmed in Figure 6. The forming process of the deep drawing process is summarized in Table 4, and the cause of the fracture range was analyzed through the forming of the drawing process.

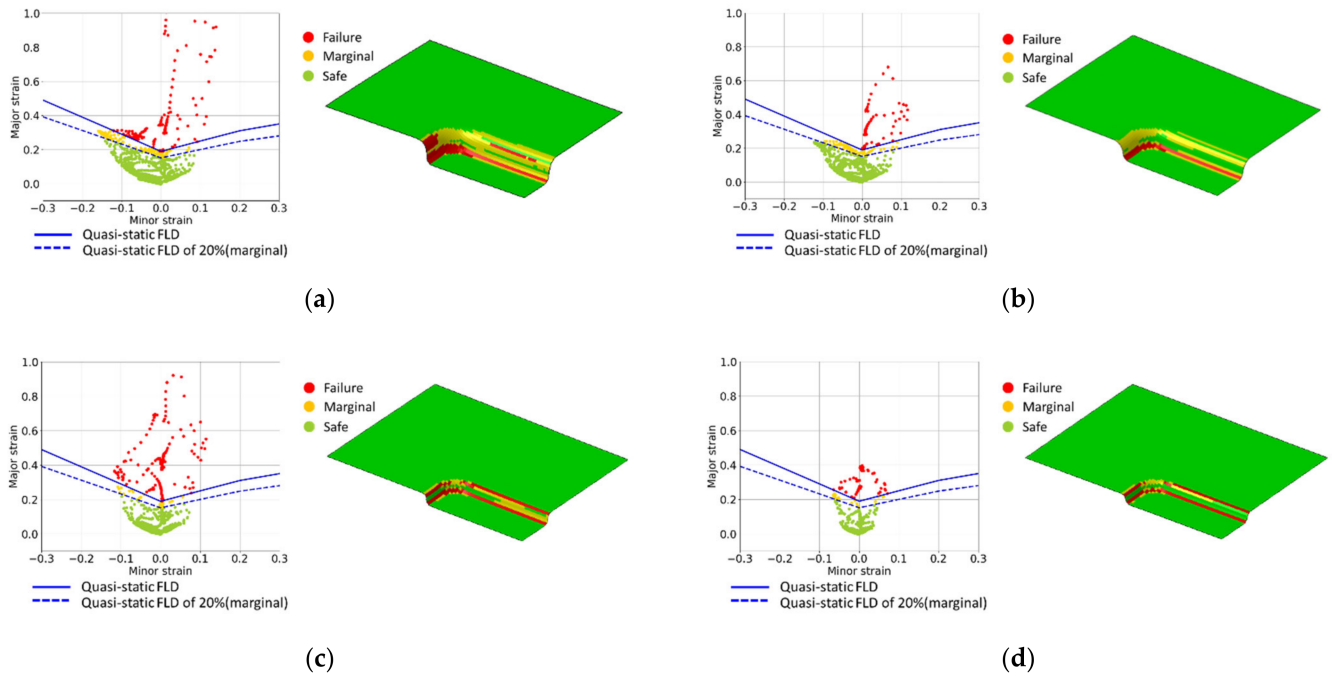


Figure 4. Final thickness of the drawing process for (a) CASE 1, (b) CASE 2, (c) CASE 3, and (d) CASE 4.

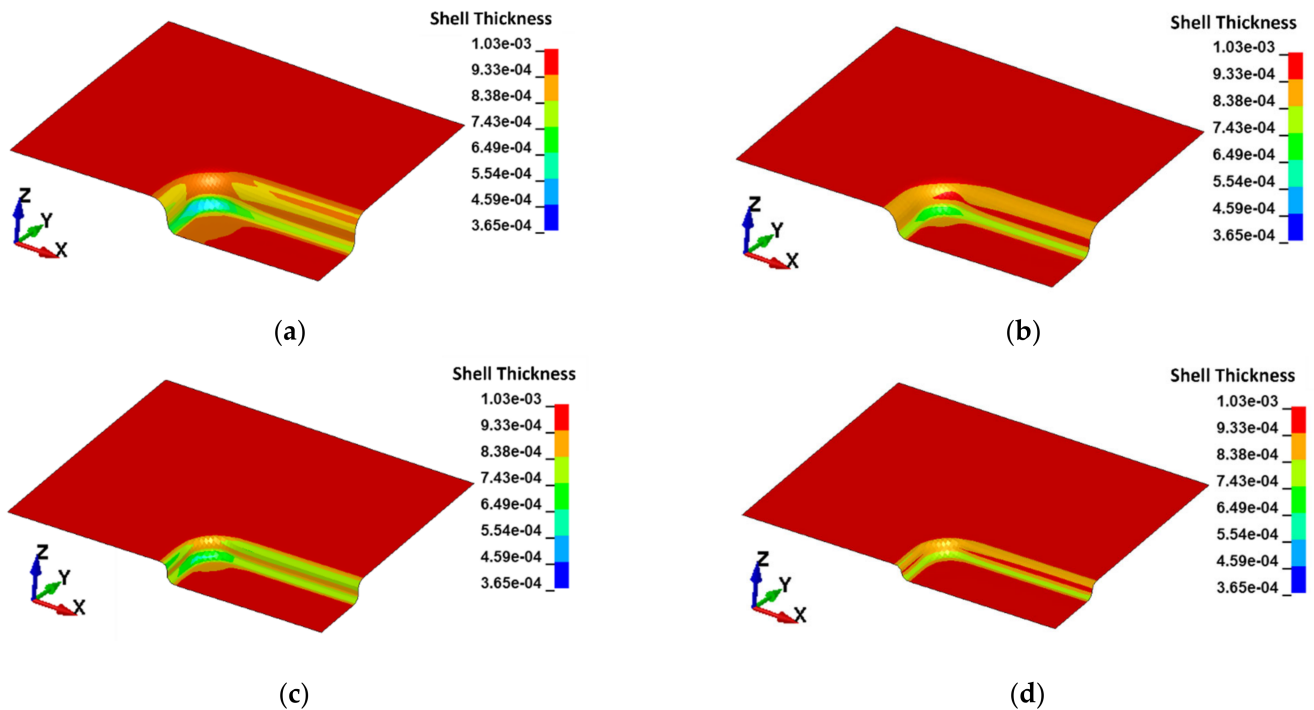


Figure 5. FLD and formability evaluation of drawing process for (a) CASE 1, (b) CASE 2, (c) CASE 3, and (d) CASE 4.

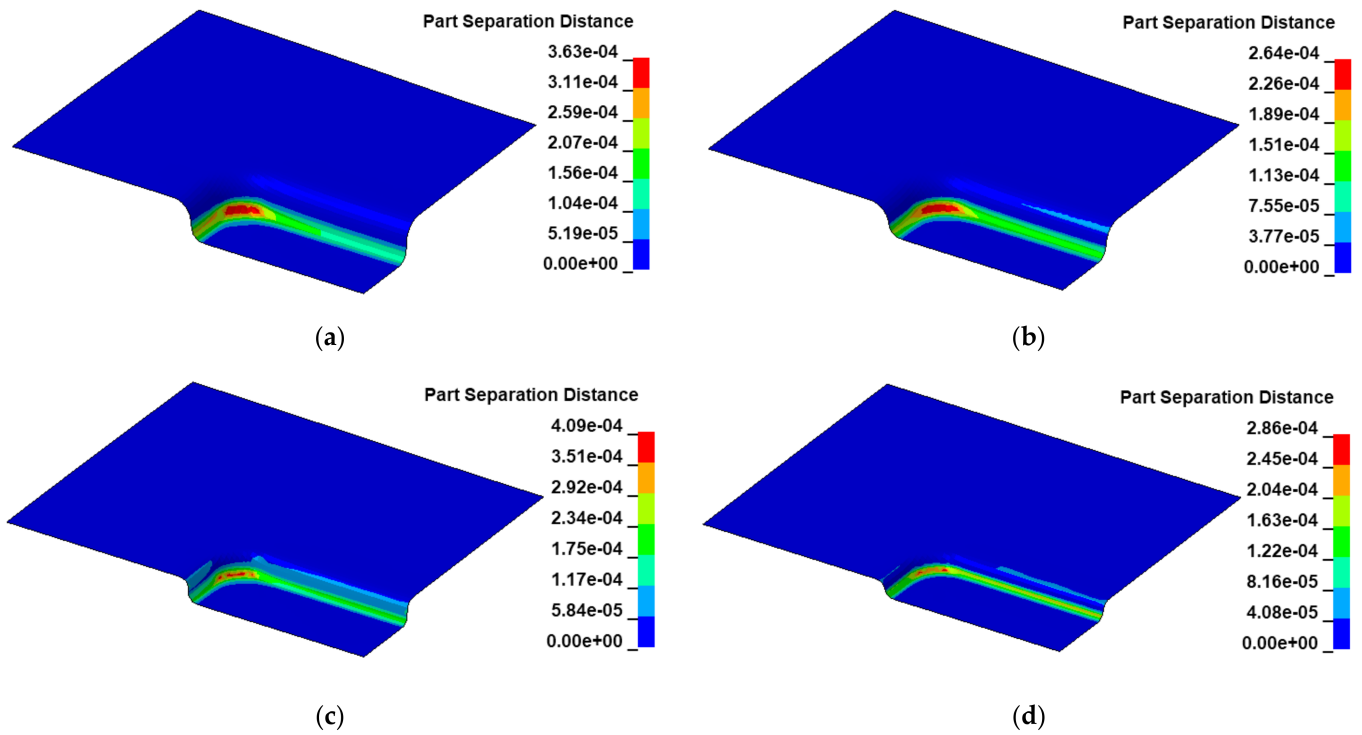
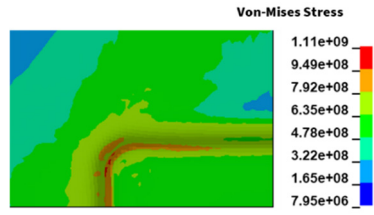
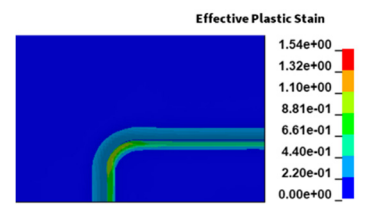


Figure 6. Distance between sheet and die (forming accuracy) for (a) CASE 1, (b) CASE 2, (c) CASE 3, and (d) CASE 4.

Table 4. Von Mises stress and effective plastic strain distribution diagram corresponding to the drawing process (CASE 1, depth 5 mm).

Time	Forming Process	Von-Mises Stress	Effective Plastic Strain
0.3 ms			
0.5 ms			
0.7 ms			

Table 4. Cont.

Time	Forming Process	Von-Mises Stress	Effective Plastic Strain
1.0 ms (end)			

Through the final thickness (Figure 4) and formability evaluation (Figure 5), it can be confirmed that the thickness reduction was higher in the die R and punch R regions, and therefore, fracture occurs in these regions. Furthermore, through Figure 5 that shows the forming accuracy, it can be seen that the final finite element analysis result of the drawing process does not perfectly match the target shape. Although it is assumed that the decrease in thickness is the main cause, Figures 4 and 6 show that perfect forming is not achieved in CASE 3 and 4 even after considering the decrease in thickness.

The causes of fracture in the die R and punch R regions were identified through the stress and strain distribution diagram during the drawing process, and the forming process for CASE 1 is summarized in Table 4. Through the forming process (Table 4), it can be seen that in the drawing process, the local area (A) of the sheet in contact with punch R leads the forming.

Due to this process, stress and strain are concentrated in the region near punch R. Deformation in the die R region is caused by tensile deformation as the sheet fixed by the die and holder proceeds with the forming process. This can be seen through the Von Mises stress distribution diagram, and the stress concentration due to the resistance to deformation in the die R region can be confirmed.

3.2. Electromagnetic Forming

To confirm the dominant strain rate in the finite element analysis of EMF, as the strain was greatest in die R, the elements of the die R region were randomly selected. It was verified that the dominant strain rate was 100,000/s or higher and the minimum strain rate was about 10,000/s. This is shown in Figure 7.

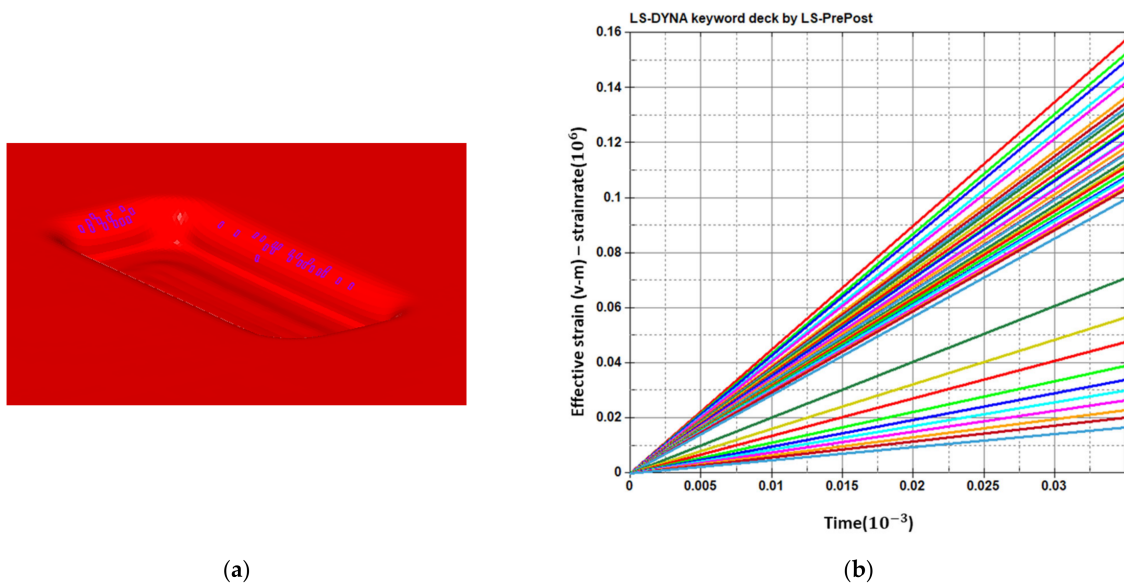


Figure 7. Strain rate for elements of die R area (a) randomly selected elements in die R region, and (b) strain rate of selected elements.

The final thickness of EMF analysis is shown in Figure 8, and the formability evaluation and FLD are shown in Figure 9. In addition, the forming accuracy and forming process of EMF are shown in Figure 10 and Table 5, respectively.

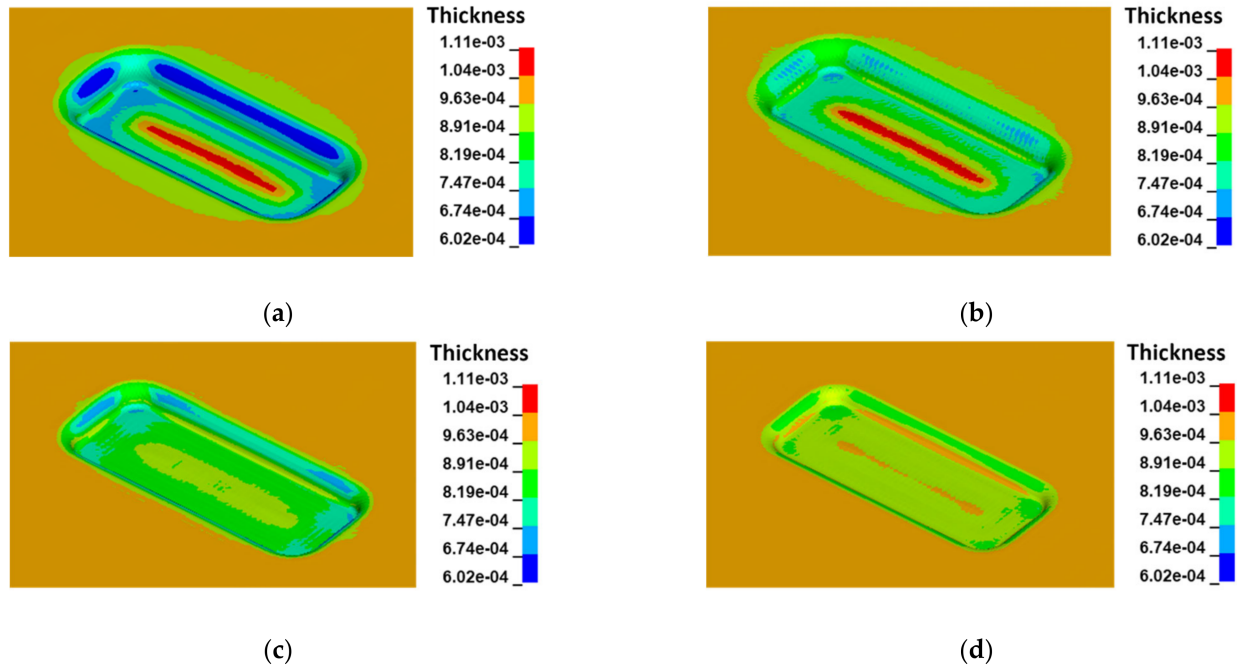


Figure 8. Final thickness of EMF for (a) CASE 1, (b) CASE 2, (c) CASE 3, and (d) CASE 4.

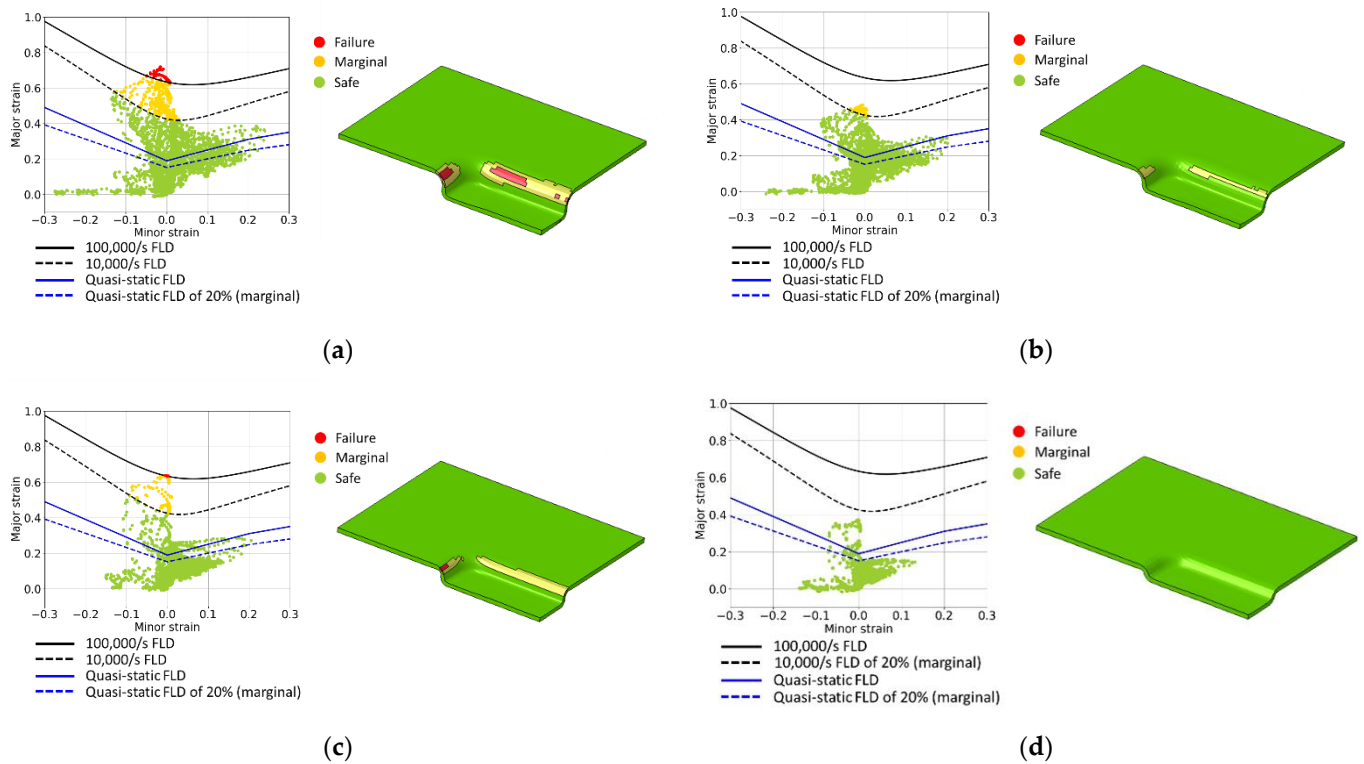


Figure 9. FLD and formability evaluation of EMF for (a) CASE 1, (b) CASE 2, (c) CASE 3, and (d) CASE 4.

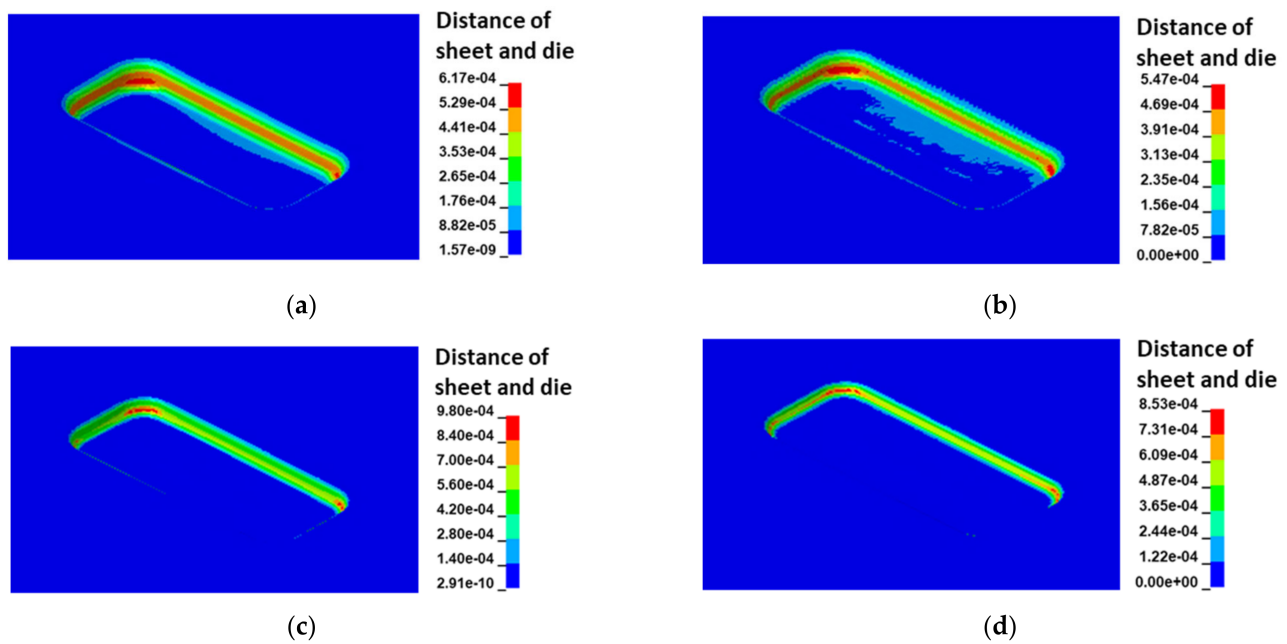


Figure 10. Distance between sheet and die (forming accuracy) for (a) CASE 1, (b) CASE 2, (c) CASE 3, and (d) CASE 4.

Table 5. Sheet inflow of each after forming.

	Drawing Process		EMF	
	X-Axis Inflow (mm)	Y-Axis Inflow (mm)	X-Axis Inflow (mm)	Y-Axis Inflow (mm)
CASE 1	0.96	1.80	0.05	0.11
CASE 2	0.62	1.20	0.06	0.12
CASE 3	0.43	0.83	0.04	0.08
CASE 4	0.19	0.10	0.02	0.04

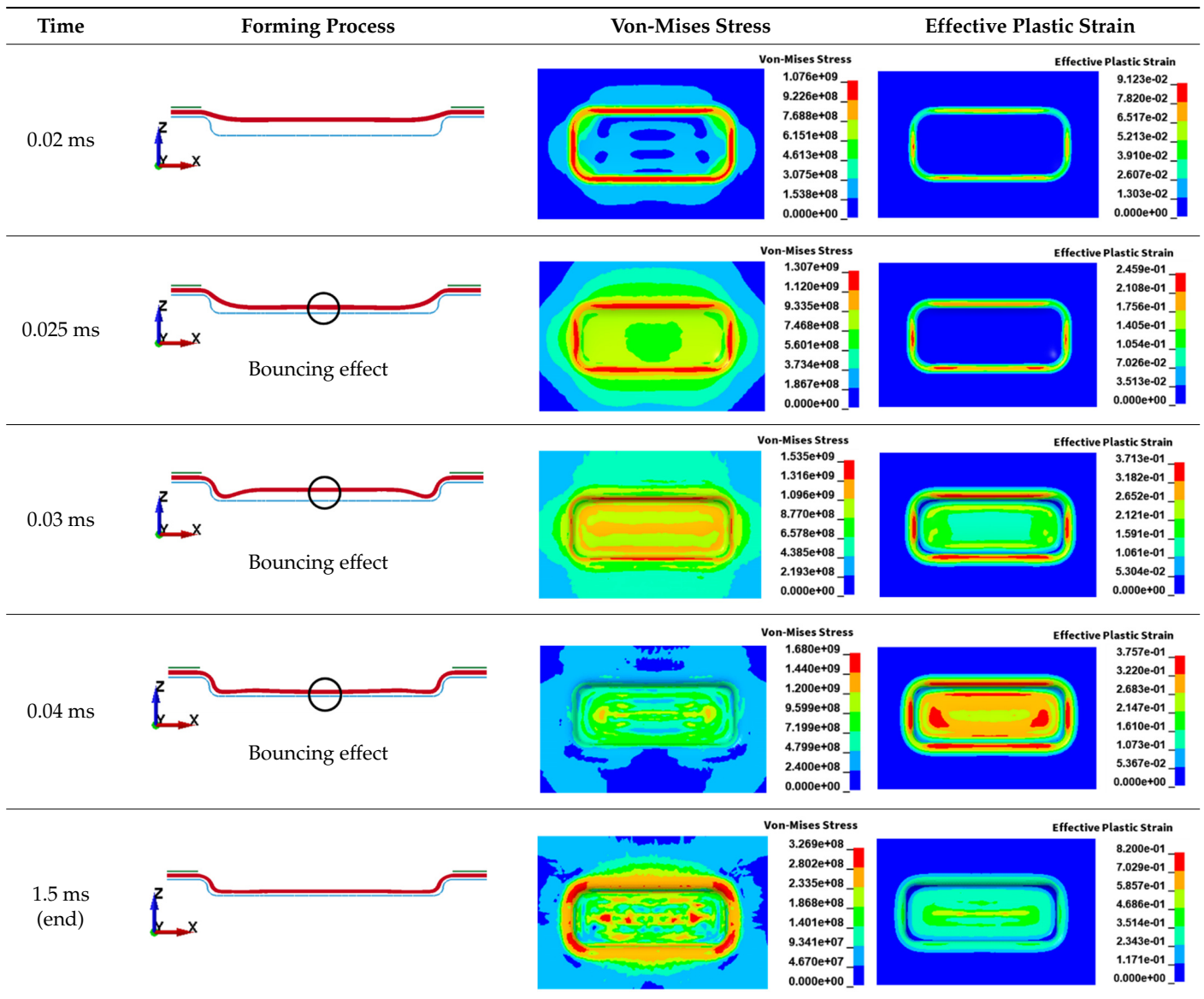
For evaluating the formability of EMF analysis, FLD values of 10,000/s and 100,000/s were applied by considering the strain rate of the EMF analysis. Since the dominant strain rate in the EMF analysis of this study was 100,000/s or higher (approximately 100,000–200,000/s), the region with a very high probability of fracture beyond this was designated as the failure region (Failure). In addition, the area expressed as marginal was an element located in the range 10,000/s to 100,000/s, and it was an area where there is a possibility of fracture with a minimum strain rate of 10,000/s or higher. Through this, it can be seen that CASE 4 does not fracture, and CASES 1–3, which have a possibility of fracture, also have a significantly reduced fracture range compared to the drawing process.

In EMF, it can be confirmed that fracture occurs at the die R. In addition, through the final thickness result of the EMF analysis, it can be seen that unlike the drawing process in which thickness reduction is concentrated in the punch R and die R regions, in EMF, deformation occurs in the entire area of the forming part. Among them, the thickness variation in the regions near die R and the central area is conspicuous. Tensile deformation occurs in the die R region, and compressive deformation occurs in the central portion. In addition, the sheet inflow in EMF is a value corresponding to 1/10 times that of drawing, which can be confirmed in Table 6. Although the EMF process has a lower sheet inflow rate than the drawing process, from Figure 8 and Table 7, it can be seen that the fracture prediction range and thickness variation are smaller than those of the drawing process.

Table 6. Minimum thickness of each case.

	CASE 1 (mm)	CASE 2 (mm)	CASE 3 (mm)	CASE 4 (mm)
Drawing process	0.365	0.563	0.648	0.714
EMF	0.602	0.694	0.712	0.793

Table 7. Von Mises stress and effective plastic strain distribution diagram corresponding to EMF (CASE 2, depth 4 mm).



Through the evaluation of formability, it was verified that EMF has advantages over the drawing process. However, it can be seen that the molding accuracy shown in Figure 10 is lower than that of the drawing process. The forming process of EMF for CASE 2 is summarized in Table 5, and the finite element analysis results of EMF were analyzed using this. The reason for choosing a case different from that of the drawing process is that among the four cases, CASE 2 illustrated the most prominent forming characteristics of EMF in the finite element analysis program. Through EMF (Table 7), it can be seen that stress and strain are concentrated in the die R region during the overall forming process. This is because a relatively uniform forming force is applied to the forming part that is not fixed by the die and holder, and forming proceeds simultaneously. In contrast, the die R region fixed by the

die and holder is stretched by the surrounding region where the forming is in progress and has a reduction in thickness.

After approximately 0.03 ms, the stress and strain are concentrated at the center of the forming part. This is because of the bouncing effect, in which the sheet formed at high speed collides with the die and bounces off. As this bouncing phenomenon is repeated, the thickness increases due to compression deformation that occurs at the center of the forming part. This phenomenon will appear as a wrinkle on the bottom surface of the actual panel.

4. Characterization of Electromagnetic Forming

Through the finite element analysis results, it was confirmed that the EMF had low accuracy with the target shape at the corner areas of the die. In addition, the deeper the target forming depth and the smaller the die R, the lower the accuracy of the target shape. To understand the cause of this, a free bulge die was applied instead of a square cup-shaped die. This is used to determine the shape that the forming coil gives the sheet. Through the free bulge finite element analysis results, the characteristics of EMF were identified by analyzing how EMF was formed. Similar to the die R of the existing case, finite element analysis was additionally performed for free bulge 1 with die R 2 mm and free bulge 2 with die R 1 mm. Then, the finite element analysis was performed by lowering the input voltage from 30 to 10 kV. The final shape of the free bulge analysis is shown in Figure 11, and the sheet is formed into a hill-like shape after EMF. Therefore, the z -axis cross-section of the free bulge has an ellipse-like final shape. In addition, through Figure 12, which presents the x -axis and y -axis sections of the final shapes of free bulges 1 and 2, the z -axis section, that is, the size of the ellipse, becomes smaller as it goes down to the final shape. Therefore, EMF causes an unformed phenomenon in the corner area, and the greater the forming depth, the lower the forming accuracy.

Comparing the final shapes of the graphs (Figure 12) of free bulges 1 and 2, free bulge 1 has a higher final molding height than free bulge 2. The final molding heights of free bulge 1 and free bulge 2 are approximately 8.8 mm and 6.5 mm, respectively, with a difference of approximately 1.3 mm. This is because of the difference in the amount of sheet inflow; more sheet inflow was seen in free bulge 1 than 2. This difference in sheet inflow is due to the following reasons. The cross-sections of the x -axis and y -axis of free bulges 1 and 2 and the amount of sheet inflow shown in Table 8 show that the final shape is determined by die R regardless of the overall shape of the die for EMF. If the die R is large, it is smoothly stretched along the curvature, forming proceeds, and the inflow of the plate material is relatively smooth. On the other hand, when the die R is small, rather than being formed along the curvature, the position of the plate is fixed while the plate is formed as if it is bent, and hence, the inflow of the plate is relatively difficult. If there is no inflow of sheet, the limit of deformation is also reduced because it deforms only with a limited sheet. Hence, the smaller the die R in the same model, the lower the forming accuracy.

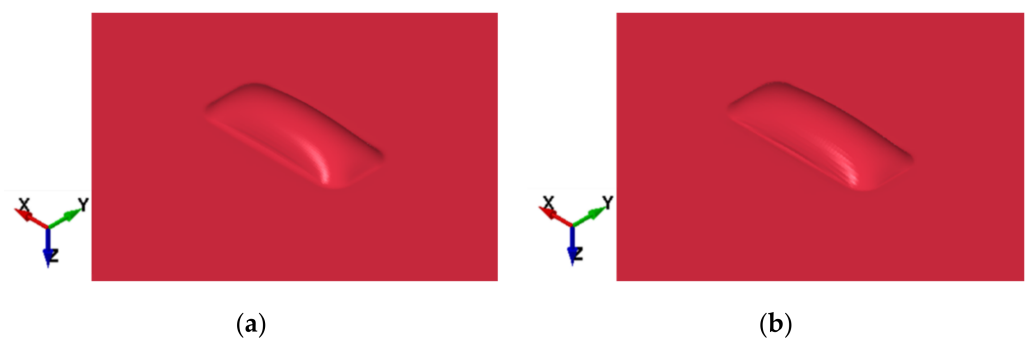


Figure 11. Final shape of free bulge model by finite element analysis for (a) free bulge 1 and (b) free bulge 2.

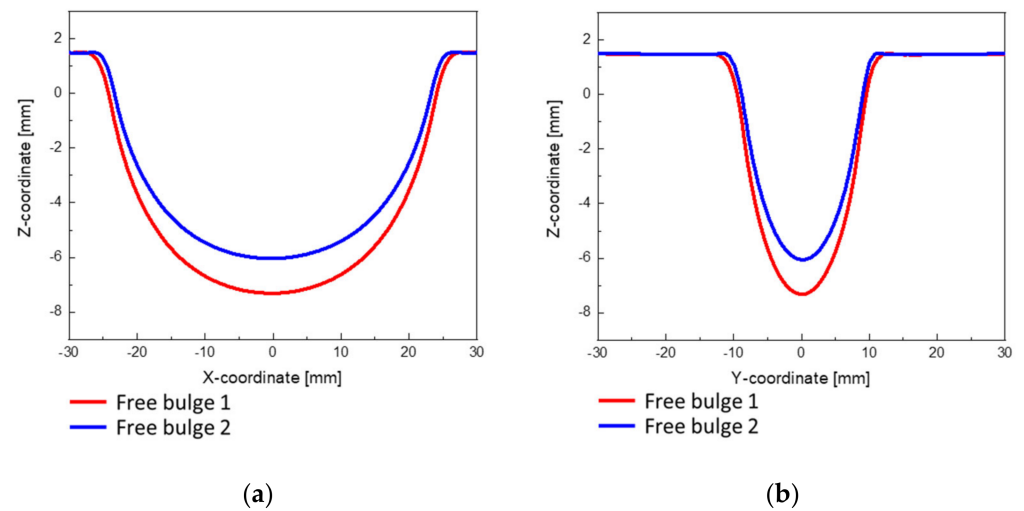


Figure 12. Graph of cross-section of free bulge models: (a) x-axis (b) y-axis.

Table 8. Cross-section and sheet inflow of free bulge models for EMF.

	X-Axis Cross-Section	Y-Axis Cross-Section	X-Axis Inflow	Y-Axis Inflow
Free bulge 1			0.12	0.28
Free bulge 2			0.11	0.19

5. Conclusions

In this study, to analyze the characteristics of EMF, finite element analysis was performed on four rectangular cup-shaped models. Through the finite element analysis results, the formability of the drawing process and EMF were compared, and the cause of the difference in the results was analyzed. The following results were obtained after the analysis:

- (1) From the finite element analysis results of deep drawing, the thickness reduction tends to be concentrated in the area in contact with the punch R and die R area. In addition, the fracture of the aforementioned area was predicted in the formability evaluation through a quasi-static forming limit diagram.
- (2) Unlike drawing, in which deformation is concentrated in a specific area, in EMF, deformation occurs relatively in the entire area of the forming part. Among them, it was confirmed that the deformation in the die R and the central part was noticeable. The primary factor for the difference between the finite element analysis results of EMF and the drawing process is the difference in the area where the forming force acts. In the drawing process, the forming force is concentrated on the local area in contact with the punch R to lead the overall forming, whereas in EMF, the forming force is applied to the entire area of the forming part, and forming is carried out at the same time.
- (3) The forming limit diagrams were used to evaluate the formability of the EMF analysis, taking into account the minimum (10,000/s) and dominant strain rates (100,000/s) of the EMF analysis. Although the sheet in flow in the EMF analysis was 1/10 of the drawing process sheet inflow, the fracture prediction range was noticeably reduced. Through this, it was confirmed that there is an advantage in moldability in high-speed molding such as EMF.
- (4) However, EMF using a spiral coil showed lower forming accuracy than the drawing process, and the unformed phenomenon in the die corner area was particularly no-

ticeable. This is because when EMF is in progress, the sheet that is formed maintains a hill-like shape. Looking at the z-axis cross-section of the free bulge final shape, the sheet has an elliptical shape, which is the reason for the low accuracy in the die corner area. In addition, the size of the z-axis cross-section decreases toward the bottom of the final shape, which is why the deeper the target depth in EMF, the lower the forming accuracy.

- (5) From the EMF finite element analysis results, it was confirmed that the smaller the die R, the lower the forming accuracy. This is because for smaller values of die R, the sheet inflow is less smooth as the sheet is formed to be bent.

In the drawing process, the area in contact with the punch leads to forming, causing local deformation. On the contrary, in the EMF, the Lorentz force acts on the entire area of the formed part, resulting in a relatively uniform deformation in the entire area. Although the amount of sheet flow in the EMF was 1/10 times that in the drawing process, the fracture prediction area showed a tendency to decrease. The EMF is formed into a dome-like shape with a uniform Lorentz force. The die and plate collide, causing bouncing; furthermore, the forming at the corner of the square cup is not perfect. Therefore, additional research is required to perfectly form a square cup shape via EMF. Based on the EMF characteristics identified in this study, a follow-up study will be conducted on the improvement method for the EMF bouncing effect and the unformed corner area. As EMF can show different results depending on the structure of the coil, it is also necessary to study the optimization of the coil structure of each process. In addition, experiments will be conducted to verify the finite element analysis results.

Author Contributions: Conceptualization, M.L., Y.S. and J.K.; software, M.L.; investigation, M.L.; resources, H.B. and Y.S.; writing-original draft preparation, M.L. and H.B.; writing-review and editing, Y.S., J.P., M.L. and J.K.; visualization, M.L.; supervision, J.K.; project administration, Y.S. and J.P.; funding acquisition, J.K. All authors have read and agreed to the published version of the manuscript.

Funding: This study was supported by the National Research Foundation of Korea (NRF) grant funded by the Korea government (MSIT) (No. 2019R1A5A6099595) and the Basic Science Research Program (No. NRF-2020R1I1A3A04036865) and the BK21 FOUR (Fostering Outstanding Universities for Research) funded by the Ministry of Education (MOE, Korea) and National Research Foundation of Korea (NRF).

Institutional Review Board Statement: Not applicable.

Informed Consent Statement: Not applicable.

Data Availability Statement: The data presented in this study are available on request to the corresponding author.

Conflicts of Interest: The authors declare no conflict of interest.

References

1. Kotra. Available online: https://dream.kotra.or.kr/kotranews/cms/news/actionKotraBoardDetail.do?SITE_NO=3&MENU_ID=180&CONTENTS_NO=1&bbsSn=243&pNttSn=189300 (accessed on 1 July 2021).
2. Hyundai Motor Group. Available online: <https://tech.hyundaimotorgroup.com/kr/article/breaking-the-rules-of-tradeoff-between-strength-and-lightweight/> (accessed on 3 December 2019).
3. Meschut, G.; Janzen, V.; Olfermann, T. Innovative and Highly Productive Joining Technologies for Multi-Material Lightweight Car Body Structures. *Mater. Eng. Perform.* **2014**, *12*, 1515–1523. [[CrossRef](#)]
4. Kim, J.; Noh, H.G.; Ko, S.J.; Kim, T.J. Analysis of Electromagnetic Forming Using Sequential Electromagnetic-Mechanical Coupled Simulations. *Trans. Mater. Process.* **2012**, *21*, 441–446. [[CrossRef](#)]
5. Psyk, V.; Risch, D.; Kinsey, B.L.; Tekkaya, A.E.; Kleiner, M. Electromagnetic forming-A review. *J. Mater. Process. Technol.* **2011**, *211*, 787–829. [[CrossRef](#)]
6. Qiu, L.; Wang, B.; Abu-Siada, A.; Xiong, Q.; Zhang, W.; Ge, W.; Liu, C.; Jiang, L.; Wang, C. Research on Forming Efficiency in Double-Sheet Electromagnetic Forming Process. *IEEE Access* **2020**, *8*, 19248–19255. [[CrossRef](#)]
7. Trzepieciński, T. Recent Developments and Trends in Sheet Metal Forming. *Metals* **2020**, *10*, 779. [[CrossRef](#)]
8. Kim, J.; Song, W.J.; Kang, B.S. Study on Formability Enhancement of Electromagnetic Forming using Gurson Plasticity Material Model. *Trans. KASE* **2013**, *21*, 98–104.

9. Chen, M.; Lai, Z.; Cao, Q.; Han, X.; Wang, C.; Liu, N.; Li, L. Improvement on formability and forming accuracy in electromagnetic forming of deep-cavity sheet metal part using a dual-coil system. *J. Manuf. Process.* **2020**, *57*, 209–221. [[CrossRef](#)]
10. Kamal, M.; Daehn, G.S. A Uniform Pressure Electromagnetic Actuator for Forming Flat Sheets. *J. Manuf. Sci. Eng.* **2006**, *129*, 369–379. [[CrossRef](#)]
11. Demir, K.; Goyal, S.; Hahn, M.; Tekkaya, E. Novel Approach and Interpretation for the Determination of Electromagnetic Forming Limits. *Materials* **2020**, *13*, 4175. [[CrossRef](#)] [[PubMed](#)]
12. Kim, H.K.; Noh, H.G.; Kang, B.S.; Kim, J. Design of a Free Bulge Test Coil Using Electromagnetic Forces and Comparison between Experimental and Numerical Results. *Trans. Mater. Process.* **2014**, *23*, 431–438. [[CrossRef](#)]
13. Woo, M.A.; Lee, S.M.; Lee, K.H.; Song, W.J.; Kim, J. Application of an Artificial Neural Network Model to Obtain Constitutive Equation Parameters of Materials in High Speed Forming Process. *Trans. Mater. Process.* **2018**, *27*, 331–338.
14. Byun, H.B.; Kim, J. Estimating Strain Rate Dependent Parameters of Cowper-Symonds Model Using Electrohydraulic Forming and Artificial Neural Network. *Trans. Mater. Process.* **2022**, *31*, 81–88.